

# Apparatus for the study of electronic spectra of collisionally cooled cations: *para*-dichlorobenzene

Anatoly Dzhonson<sup>a</sup>, Dieter Gerlich<sup>b</sup>, Evan J. Bieske<sup>c</sup>, John P. Maier<sup>a,\*</sup>

<sup>a</sup> Department of Chemistry, University of Basel, Klingelbergstrasse 80, Basel CH-4056, Switzerland

<sup>b</sup> Fakultät für Naturwissenschaften, TU Chemnitz, Straße der Nationen 62, D-0911, Germany

<sup>c</sup> School of Chemistry, University of Melbourne, Parkville, 3010 Vic., Australia

Received 10 October 2005; received in revised form 26 November 2005; accepted 28 November 2005

Available online 17 April 2006

## Abstract

An apparatus has been developed with the aim of measuring the electronic spectra of large ions at low vibrational and rotational temperatures, as of relevance to astronomical observations. The mass-selected ions are injected into a 22-pole radio frequency trap where internal degrees of freedom are deactivated by cryogenically cooled helium gas. In these first experiments the electronic transitions are detected by a predissociation process for  $\text{N}_2\text{O}^+$  and *para*-dichlorobenzene cations (*p*-DCB<sup>+</sup>).

In case of  $\text{N}_2\text{O}^+$  the  $\tilde{A}^2\Sigma^+ \leftarrow \tilde{X}^2\Pi_{3/2}$  transition is rotationally resolved and the population fits to  $T_{\text{rot}} \sim 25$  K. The  $\tilde{B}^2B_{3u} \leftarrow \tilde{X}^2B_{2g}$  system of *p*-DCB<sup>+</sup> shows narrow vibronic bands and an absence of hot bands indicating that the rotational and vibrational degrees of freedom have been relaxed. The vibrational structure has been assigned leading to the frequencies of several of the modes in the  $\tilde{B}^2B_{3u}$  state. The dynamics of the photon absorption/dissociation are discussed.

© 2006 Elsevier B.V. All rights reserved.

**Keywords:** Electronic spectra; Cold-cations; Ion-trap

## 1. Introduction

A significant challenge remains the measurement of the electronic spectra of large molecular ions in the gas phase and at low internal temperature. Problems include low ion densities and spectral congestion due to the presence of species with overlapping absorptions and vibrational hot bands. Sometimes it is feasible to generate sufficient densities of molecular ions in a plasma or discharged supersonic expansion so that laser absorption, laser induced fluorescence, or cavity ringdown spectra can be recorded. However, due to the chemical complexity of plasma environments there are often difficulties in associating spectral features with a particular molecular species.

An alternative approach to obtaining electronic spectra is by resonance enhanced photodissociation, exposing the molecular ions to a tuneable laser beam in a tandem mass spectrometer while detecting photofragment ions as a function of laser wavelength. The advantages are that the parent molecular ions

and photofragments can be mass-selected removing any ambiguity in their identity, and that the photofragments can be detected with almost unit efficiency conferring high sensitivity. In some cases, such as  $\text{N}_2\text{O}^+$ , it is possible to access predissociative rovibronic states through the absorption of a single visible or UV photon. Alternatively, if a single photon does not provide sufficient energy to fragment the molecule it is possible that absorption of multiple photons will. For example, many organic ions undergo rapid internal conversion from excited electronic states, yielding vibrationally hot ions in the ground electronic state. If the vibrational energy exceeds the fragmentation threshold, the ions can dissociate. Otherwise, the absorption/internal conversion process can continue until the ions have sufficient energy to dissociate.

The resonance enhanced photodissociation approach has been used for many years employing a variety of different mass spectrometers and ion traps [1]. One common difficulty is that the molecular ions have considerable internal energy due to the violence of the ionisation process, so that the electronic spectra are congested and difficult to interpret. This is a particular problem for larger molecules. In order to circumvent this difficulty an apparatus has been developed in which the ions' rotational and vibrational degrees of freedom are deactivated

\* Corresponding author. Tel.: +41 61 267 38 26; fax: +41 61 267 38 55.

E-mail address: [j.p.maier@unibas.ch](mailto:j.p.maier@unibas.ch) (J.P. Maier).

by helium buffer gas collisions in a cryogenically cooled 22-pole radio frequency trap. In this paper the technique's advantages are illustrated by presenting the rotationally resolved  $\tilde{A}^2\Sigma^+ \leftarrow \tilde{X}^2\Pi_{3/2}$  spectrum of  $\text{N}_2\text{O}^+$  and the vibrationally resolved  $\tilde{B}^2B_{3u} \leftarrow \tilde{X}^2B_{2g}$  spectrum of the  $p\text{-DCB}^+$  radical cation. Both molecular ions have been subject to previous studies. The  $\text{N}_2\text{O}^+$  cation is well understood having been investigated extensively through optical emission [2], lifetime [3], and photodissociation studies [4–6]. Previously, the  $\text{N}_2\text{O}^+ \tilde{A}^2\Sigma^+ \leftarrow \tilde{X}^2\Pi_{3/2}$  electronic spectrum has been obtained by detecting the  $\text{NO}^+$  fragment, a strategy that is effective because the higher vibronic levels of the  $\tilde{A}^2\Sigma^+$  state are predissociative and lead to production of  $\text{NO}^+$  and O atom fragments. For the  $1^2$  level of the  $\tilde{A}^2\Sigma^+$  state, which is accessed in the current study, around 16% of the molecules fluoresce with the remainder dissociating [3].

The  $p\text{-DCB}^+$  radical cation was investigated initially using the techniques of photoelectron and emission spectroscopies in a molecular beam [7], and later by absorption in the rare gas matrixes [8,9]. From pulsed electron beam excitation and emission intensity measurements it has been estimated that the internal conversion rate is  $\approx 10^{11} \text{ s}^{-1}$  [7]. As discussed in the latter article, fluorescence from the  $\tilde{B}^2B_{3u} v=0$  level is weak, a situation attributed to rapid internal conversion mediated by coupling with the  $\tilde{C}^2B_{2u}$  state. The current study is the first time that a high-resolution gas-phase spectrum has been reported.

## 2. Experimental methods

The apparatus consists of an electron impact ion source, a quadrupole mass filter for selecting the desired molecular ion, a cryogenically cooled RF 22-pole trap, a second quadrupole mass filter for selecting the charged photofragments, and a Daly detector [10].

The 22-pole trap, which follows the design of Gerlich [11,12], consists of 22 stainless steel rods (1 mm diameter, 36 mm length) equally spaced on an inscribed radius of 10 mm. The rods are alternately connected to the two outputs of the RF generator. The rod assembly is enclosed by a copper box mounted on the second stage of a closed cycle helium cryostat. A thin sapphire plate (mounted with a foil of indium) conducts heat between the trap housing and the cold head. Electrical connection wires and the helium buffer gas line are precooled on the first stage of the cryostat to a temperature of 50 K before attachment to the trap. A calibrated silicon diode mounted in the base of the 22-pole trap housing was used to measure the temperature. The lowest achievable temperature is slightly above 5 K. The trap operating frequency was in the 1.5–2 MHz range while the RF amplitude was 110 V for  $p\text{-DCB}^+$  and 70 V for  $\text{N}_2\text{O}^+$ . With these parameters the depth of the effective trap potential was 20–100 meV. The 22-pole trap has a confining potential that has approximate cylindrical symmetry, and which rises steeply near the periphery (with an  $R^{20}$  dependence) leading to a large field free volume where the ions are largely unaffected by RF heating and can be effectively thermalised by helium buffer gas cooling.

The helium pressure in the region surrounding the trap was measured as  $\approx 10^{-4}$  mbar. The pressure in the trap was at least 5 times higher and was estimated as  $5 \times 10^{-4}$  mbar corresponding to a helium number density of  $4 \times 10^{14} \text{ cm}^{-3}$  at 10 K. Assuming a Langevin rate coefficient of  $\approx 10^{-9} \text{ cm}^3 \text{ s}^{-1}$ , bimolecular thermalising collisions occur at a frequency of  $\approx 4 \times 10^5 \text{ s}^{-1}$ . Therefore the ion temperature is expected to approach the ambient trap temperature in a few milliseconds. The ions remain at a slightly higher temperature than the helium buffer gas due to weak RF heating [13].

The ion source is a low-pressure electron impact device. Sample vapours are admitted to the ionisation region through a needle valve. The ionising electrons' energy was adjusted to be slightly above the target molecule's ionisation potential, 12–13 eV for  $\text{N}_2\text{O}^+$  and 9–10 eV for  $p\text{-DCB}^+$ .

The apparatus is run in a pulsed mode. Ions generated by the source are mass selected by the first quadrupole and are accumulated in the 22-pole trap for 10 ms through collisions with  $\approx 10^{-4}$  mbar helium buffer gas. Following this, the potential of an electrostatic lens at the exit of the ion source is raised preventing more ions from reaching the trap. The trapped ions are collisionally cooled by the helium buffer gas in the 22-pole trap for 70 ms before being exposed to a pulse of tuneable radiation from the OPO. Then the potential of the exit lens of the trap is lowered for 10 ms allowing the ions to exit through the second quadrupole mass filter, which is set to the mass of the photofragment ions. The latter are eventually detected by a Daly detector, the output of which is sent to a discriminator and pulse counter. Typically,  $5\text{--}10 \times 10^4$  ions are trapped and irradiated on each cycle. The light source is either the fundamental (for  $p\text{-DCB}^+$ ) or doubled (for  $\text{N}_2\text{O}^+$ ) output of a Nd:YAG pumped OPO with a bandwidth of  $\approx 0.5 \text{ cm}^{-1}$  operating at 10 Hz. The laser beam passes along the axis of the quadrupoles and 22-pole trap. The background fragment count (without laser light) was usually  $< 10$  per cycle.

## 3. Results and discussion

### 3.1. $\text{N}_2\text{O}^+$

The  $\tilde{A}^2\Sigma^+ \leftarrow \tilde{X}^2\Pi_{3/2}$  band of  $\text{N}_2\text{O}^+$  is shown in Fig. 1. Also shown are simulated spectra for temperatures of 15, 25 and 35 K [14,15]. Molecular constants used in the simulations are  $B'' = 0.41157 \text{ cm}^{-1}$ ,  $D'' = 0.2985 \times 10^{-6} \text{ cm}^{-1}$ ,  $q'' = 1.13 \times 10^{-3} \text{ cm}^{-1}$ ,  $A'' = 132.434 \text{ cm}^{-1}$ ,  $B' = 0.42893 \text{ cm}^{-1}$ ,  $D' = 0.2855 \times 10^{-6} \text{ cm}^{-1}$ , and  $\gamma'' = 7.0 \times 10^{-4} \text{ cm}^{-1}$  and are taken from [5,6]. It is apparent that the experimental spectrum corresponds well to the  $T = 25 \text{ K}$  simulated spectrum indicating that the  $\text{N}_2\text{O}^+$  ions' rotational degrees of the freedom are effectively cooled by collisions with the helium buffer gas. In principle it is also possible to assess the translational temperature of the  $\text{N}_2\text{O}^+$  ions through the Doppler broadening of the rovibronic lines. However, in the present case this was not possible because the bandwidth of the OPO radiation ( $\approx 0.5 \text{ cm}^{-1}$ ) was much greater than anticipated Doppler broadening ( $\approx 0.017 \text{ cm}^{-1}$  at 25 K).

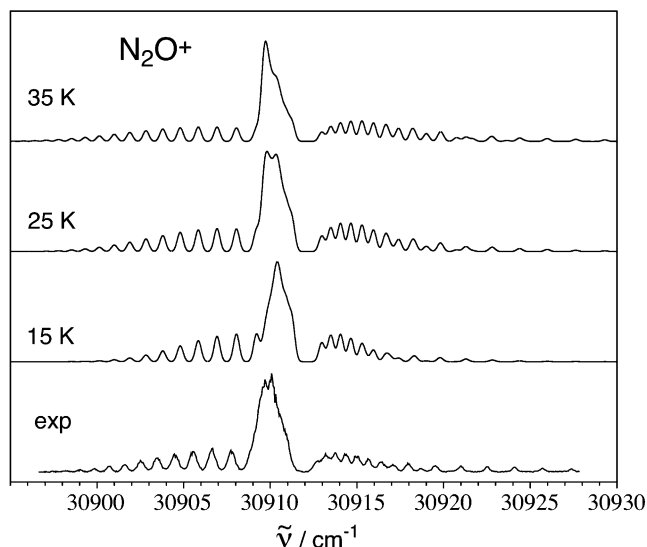


Fig. 1. The  $\tilde{A}^2\Sigma^+ \leftarrow \tilde{X}^2\Pi_{3/2} 1_0^2$  spectrum of  $\text{N}_2\text{O}^+$  obtained by monitoring the  $\text{NO}^+$  fragment count as a function of photon wavelength. Also shown are simulated spectra for temperatures of 15, 25 and 35 K.

### 3.2. para-Dichlorobenzene cation

As a second test of the apparatus the spectrum of the  $p\text{-DCB}^+$  radical cation was measured over the 19,100–22,700  $\text{cm}^{-1}$  range by monitoring the  $\text{C}_6\text{H}_4\text{Cl}^+$  fragment (i.e. Cl loss channel). The resulting spectrum, shown in Fig. 2, exhibits a series of well-resolved vibronic bands that can mainly be assigned to the dipole allowed  $\tilde{B}^2B_{3u} \leftarrow \tilde{X}^2B_{2g}$  transition. The excellent signal to noise ratio achieved is evident in Fig. 2. The lower frequency bands, which have widths of  $\approx 10 \text{ cm}^{-1}$ , have peak intensities that are  $10^3$  larger than the background level ( $\approx 10$  counts/laser shot).

The lowest frequency transition, the  $\tilde{B}^2B_{3u} \leftarrow \tilde{X}^2B_{2g} 0_0^0$  band, is observed at 19,622  $\text{cm}^{-1}$ , in excellent agreement with the value derived from the optical emission spectrum of  $p\text{-DCB}^+$  (19,620  $\pm 10 \text{ cm}^{-1}$ ) where the band was much broader [7]. For  $p\text{-DCB}^+$  [8,9,16] the corresponding  $0_0^0$  transition occur at 19,452 and 19,212  $\text{cm}^{-1}$  in Ne and Ar

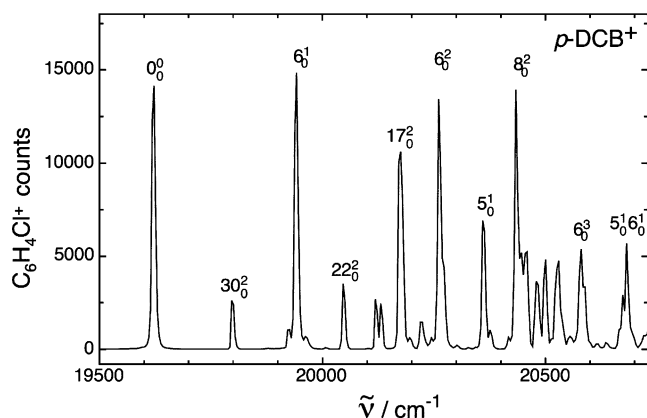


Fig. 2. The  $\tilde{B}^2B_{3u} \leftarrow \tilde{X}^2B_{2g}$  transition of the  $p\text{-DCB}^+$  radical cation over the 19,500–20,700  $\text{cm}^{-1}$  range obtained by monitoring the  $\text{C}_6\text{H}_4\text{Cl}^+$  fragment count. Wavenumbers and assignments for vibronic bands are given in Table 1.

Table 1  
Wavenumbers of vibronic bands for the  $\tilde{B}^2B_{3u} \leftarrow \tilde{X}^2B_{2g}$  system of the  $p\text{-DCB}^+$  radical cation

Band wavenumber ( $\text{cm}^{-1}$ )	Relative to $0_0^0$ ( $\text{cm}^{-1}$ )	Assignment
19,622	0	$0_0^0$
19,797	175	$30_0^2$
19,942	320	$6_0^1$
20,046	424	$22_0^2$
20,118	496	$6_0^1 30_0^2$
20,130	508	$29_0^1 30_0^1$
20,175	553	$17_0^2$
20,219	597	
20,260	638	$6_0^2$
20,270	648	$27_0^2$
20,359	737	$5_0^1$
20,434	812	$8_0^2$
20,459	837	$29_0^2$
20,479	857	$16_0^1 17_0^1$
20,500	878	$6_0^1 17_0^2$
20,530	908	
20,580	958	$6_0^3$
20,682	1060	$5_0^1 6_0^1/4_0^1$

matrices respectively, representing matrix induced red shifts of 0.9 and 2.1%, respectively.

Wavenumbers and assignments for the lower energy  $\tilde{B}^2B_{3u} \leftarrow \tilde{X}^2B_{2g}$  transitions are listed in Table 1. Assignments were made on the basis of a comparison between the experimental frequencies of neutral  $p\text{-DCB}$ , and with Ar matrix absorption and gas-phase emission spectra of  $p\text{-DCB}^+$ . The prominent 320  $\text{cm}^{-1}$  progression, which was also observed in Ar matrix absorption spectra with a similar spacing (320 and 331  $\text{cm}^{-1}$ ) [8,9], corresponds to the  $\nu_6(a_{1g})$  vibration (symmetric C–Cl stretch). The enhanced spectral resolution and excellent S/N of the gas phase spectrum compared to the earlier Ar matrix absorption spectra allow us to identify a number of previously unobserved vibronic transitions including  $30_0^2$ ,  $22_0^2$ ,  $6_0^1 30_0^2$ ,  $29_0^1 30_0^1$ ,  $17_0^2$ ,  $5_0^1$ ,  $8_0^2$ ,  $29_0^2$ ,  $16_0^1 17_0^1$  and  $5_0^1 6_0^1$ . Vibrational frequencies for the  $\tilde{B}^2B_{3u}$  state based on these transitions, along with corresponding values for the  $S_0$  and  $S_1$  states of the neutral  $p\text{-DCB}$  are given in Table 2. In most cases, the  $p\text{-DCB}^+$   $\tilde{B}^2B_{3u}$  state frequencies are similar to those of the neutral  $p\text{-DCB}$  molecule.

The  $p\text{-DCB}^+$  spectrum becomes congested above 21,000  $\text{cm}^{-1}$  (Fig. 3) where the  $\tilde{C}^2B_{2u} \leftarrow \tilde{X}^2B_{2g}$  transition is predicted to occur [7]. Although dipole forbidden it may be induced through vibronic coupling between the  $\tilde{C}^2B_{2u}$  and  $\tilde{B}^2B_{3u}$  states. The only mode with appropriate symmetry to couple the two states is the  $\nu_9(b_{1g})$  vibration which has a frequency of 815  $\text{cm}^{-1}$  in neutral  $p\text{-DCB}$ . From the photoelectron spectrum, the  $\tilde{C}^2B_{2u}$  state was estimated to lie 1045  $\text{cm}^{-1}$  above the  $\tilde{B}^2B_{3u}$  state. It is also possible that it lies somewhat lower in energy and is effectively isoenergetic with the  $\tilde{B}^2B_{3u}$  state [7].

The  $p\text{-DCB}^+$  photofragmentation process is now considered. A strong photodissociation signal into  $\text{C}_6\text{H}_4\text{Cl}^+$  is

Table 2  
Selected vibrational frequencies bands for the  $S_0$  and  $S_1$  states of neutral  $p$ -DCB and for the state of the  $p$ -DCB<sup>+</sup> radical cation

Mode	Neutral $p$ -DCB $S_0^a$	Neutral $p$ -DCB $S_1^b$	$p$ -DCB <sup>+</sup> $\tilde{B}^2B_{3u}$ Ar matrix	$p$ -DCB <sup>+</sup> $\tilde{B}^2B_{3u}$ this work	Description
5 ( $a_g$ )	747	727		737	Ring def.
6 ( $a_g$ )	328	301	320 <sup>c</sup> 331 <sup>d</sup>	320	Symmetric C–Cl stretch
8 ( $a_u$ )	405	167		406	Ring twist
16 ( $b_{2g}$ )	687	416		581	Ring twist
17 ( $b_{2g}$ )	298			276	Out of plane C–Cl bend
22 ( $b_{2u}$ )	226	225		212	In plane C–Cl bend
26 ( $b_{3g}$ )	626	538			Ring def.
27 ( $b_{3g}$ )	350	339		324	In plane C–Cl bend
29 ( $b_{3u}$ )	485	294		420	Ring twist
30 ( $b_{3u}$ )	122	75		88	Out of plane C–Cl bend

<sup>a</sup> Ref. [19].

<sup>b</sup> Ref. [20,21].

<sup>c</sup> Ref. [8].

<sup>d</sup> Ref. [9].

observed when the laser is tuned to the  $\tilde{B}^2B_{3u} \leftarrow \tilde{X}^2B_{2g}$  band origin ( $19,622 \text{ cm}^{-1} \approx 2.4 \text{ eV}$ ) despite the fact that the energetic threshold for the process has been determined as  $3.32 \pm 0.18 \text{ eV}$  [16], around 0.9 eV above the  $\tilde{B}^2B_{3u} \leftarrow \tilde{X}^2B_{2g}$  band origin. The possibility that the  $p$ -DCB<sup>+</sup> cations absorb but a single photon and already possess sufficient internal energy to make up the deficit and take them above the fragmentation threshold is unlikely given that very sharp vibronic bands are observed in the lower energy part of the spectrum and because of the absence of vibrational hot bands. The most likely explanation is that the photofragmentation process involves the absorption of two photons from the same 10 ns laser pulse (Fig. 4).

Absorption of two photons from one laser pulse could occur in a sequential photo-absorption/internal conversion cycle illustrated in Fig. 4. Resonant excitation of a  $\tilde{B}^2B_{3u} \leftarrow \tilde{X}^2B_{2g}$  transition yields, through internal conversion, highly vibrationally excited  $\tilde{X}^2B_{2g}$  state ions, which in turn absorb a second photon of the same frequency to produce vibrationally energized  $\tilde{B}^2B_{3u}$  state ions, which then internally convert to

produce  $\tilde{X}^2B_{2g}$  ions with  $\approx 4.8 \text{ eV}$  of vibrational energy. The second absorption step would access state levels with 2.4 eV of vibrational energy where the density of vibrational states is high. This sequential process seems feasible given that very rapid internal conversion from the  $\tilde{B}^2B_{3u}$   $0^0$  level has been deduced from emission studies ( $k_{ic} \approx 10^{11} \text{ s}^{-1}$ ) [7]. Internal conversion for higher  $\tilde{B}^2B_{3u}$  vibronic levels is likely to be even more rapid. Based on the coincidence measurements,  $p$ -DCB<sup>+</sup> ions with  $E_{vib} = 4.8 \text{ eV}$  would dissociate at rates of  $10^4$ – $10^5 \text{ s}^{-1}$  (i.e. on timescales  $< 1 \text{ ms}$ ) [17].

It is interesting to note that the Ar matrix  $\tilde{B}^2B_{3u} \leftarrow \tilde{X}^2B_{2g}$  absorption spectrum is dominated by the  $0_0^0$  band and the  $\nu_6$  progression, with the  $6_0^n$  intensities dropping as  $n$  increases. While the  $0_0^0$  and  $6_0^n$  bands also occur in the gas phase photodissociation spectrum, other transitions that might be expected to have much lower Franck-Condon factors, such as the  $22_0^2$ ,  $17_0^2$ , and  $8_0^2$  bands, also appear with comparable intensities. Furthermore, the photodissociation spectrum becomes increasingly congested above  $21,000 \text{ cm}^{-1}$  with sharp peaks protruding from a broad intense background. There are several possible causes for the intensity differences in

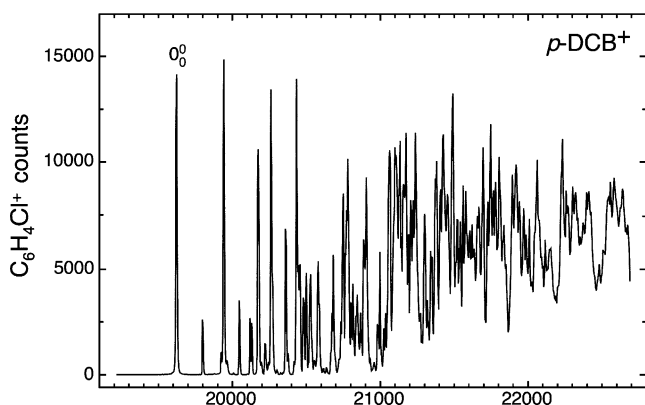


Fig. 3. Spectrum of the  $p$ -DCB<sup>+</sup> radical cation over the  $19,100$ – $22,700 \text{ cm}^{-1}$  range obtained by monitoring the  $\text{C}_6\text{H}_4\text{Cl}^+$  fragment count as a function of photon wavelength. Transitions in the  $19,600$ – $20,700 \text{ cm}^{-1}$  range can be assigned to the dipole allowed  $\tilde{B}^2B_{3u} \leftarrow \tilde{X}^2B_{2g}$  system, while above  $21,000 \text{ cm}^{-1}$  there are probably also contributions from vibronically induced  $\tilde{C}^2B_{2u} \leftarrow \tilde{X}^2B_{2g}$  transitions.

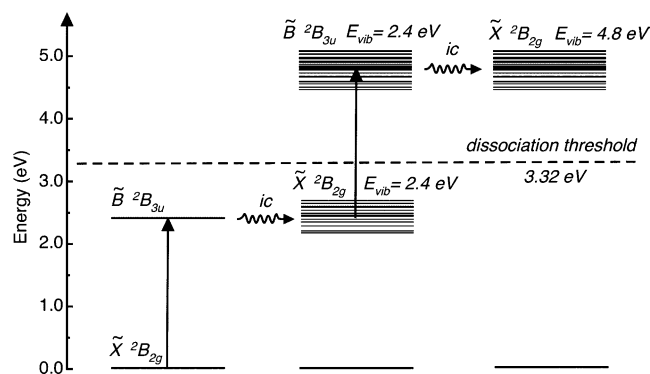


Fig. 4. Scheme for two-photon dissociation of the  $p$ -DCB<sup>+</sup> radical cation via the  $\tilde{B}^2B_{3u} \leftarrow \tilde{X}^2B_{2g}$  system. Each photon absorption is followed by rapid internal conversion to vibrationally excited levels of the  $\tilde{X}^2B_{2g}$  state. Absorption of two photons is sufficient to exceed the threshold for fragmentation into  $\text{C}_6\text{H}_4\text{Cl}^+ + \text{Cl}$ .

the matrix and resonant two photon photodissociation spectra. The most important effect is probably saturation of the first  $\tilde{B}^2B_{3u} \leftarrow \tilde{X}^2B_{2g}$  absorption step due to high laser powers so that the intensities of Franck-Condon weak transitions are boosted. Secondly, as the laser frequency is increased and higher vibronic levels are accessed in the  $\tilde{B}^2B_{3u}$  manifold in the first absorption step, the second photon absorption step will be to higher energies in the  $\tilde{B}^2B_{3u}$  manifold where the density of vibrational states is larger (see Fig. 4). For this reason it is more likely that a second photon will be absorbed and that the molecules will dissociate yielding a detectable fragment signal. If this is the case, the consequence would be that the intensities of the higher frequency  $\tilde{B}^2B_{3u} \leftarrow \tilde{X}^2B_{2g}$  vibronic bands would be enhanced relative to the lower ones.

The sharp, narrow bands observed for the  $\tilde{B}^2B_{3u} \leftarrow \tilde{X}^2B_{2g}$  system in the current study can be contrasted with the broad features observed for the  $\tilde{E} \leftarrow \tilde{X}^2B_{2g}$  system of uncooled  $p$ -DCB<sup>+</sup> radical cations in a RF ion trap over the 312–327 nm range [18]. The spectrum obtained by monitoring C<sub>6</sub>H<sub>3</sub><sup>+</sup> photofragments showed a single broad feature (fwhm  $\approx 200$  cm<sup>-1</sup>), which corresponds to the  $\tilde{E} \leftarrow \tilde{X}^2B_{2g} 0_0^0$  transition observed in the Ar matrix, superimposed on a broad background. The helium buffer gas cooling is presumably responsible for the far narrower vibronic bands (fwhm  $\approx 8$  cm<sup>-1</sup>) observed using our apparatus.

#### 4. Conclusion

The apparatus was developed primary to study the electronic spectra of large organic ions, which may be of astronomical relevance. In order to obtain and compare the laboratory electronic absorption spectra with interstellar absorptions, the internal degrees of the ions have to be cooled to temperatures appropriate to interstellar space, 20–100 K. This has been achieved as the recorded electronic spectra of N<sub>2</sub>O<sup>+</sup> and  $p$ -DCB<sup>+</sup> demonstrate. In case of N<sub>2</sub>O<sup>+</sup> the rotational temperature achieved is 25 K and for  $p$ -DCB<sup>+</sup> the narrowness of the vibronic bands and the absence of hot bands shows that the vibrational degrees of freedom have been cooled to comparable temperatures. The resulting absorption spectrum of the  $p$ -DCB<sup>+</sup>, rich in vibronic structure, can be assigned to

numerous modes in the excited state and their frequencies are inferred. The photofragment spectrum is a result of absorption of two photons in a process involving sequential internal conversion.

#### Acknowledgements

This project has been supported by the Swiss National Science Foundation (No. 200020-100019). Dr T. Schmidt (now at Sydney University) and Dr P. Kolek (now at Krakow University) are thanked for their help at the initial stages of the instrument's construction.

#### References

- [1] R.C. Dunbar, in: T.A. Miller, V.E. Bondybey (Eds.), *Molecular Ions: Spectroscopy, Structure, and Chemistry*, North-Holland, Amsterdam, 1983, p. 231.
- [2] J.H. Callomon, F. Creutzberg, *Philos. Trans. R. Soc. Lond.* 277 (1974) 157.
- [3] D. Klapstein, J.P. Maier, *Chem. Phys. Lett.* 83 (1981) 590.
- [4] R.G. Orth, R.C. Dunbar, *J. Chem. Phys.* 66 (1977) 1616.
- [5] R. Frey, R. Kakoschke, E.W. Schlag, *Chem. Phys. Lett.* 93 (1982) 227.
- [6] M. Larzilliere, C. Jungen, *Mol. Phys.* 67 (1989) 807.
- [7] J.P. Maier, O. Marthaler, *Chem. Phys.* 32 (1978) 419.
- [8] R.S. Friedman, B.J. Kelsall, L. Andrews, *J. Phys. Chem.* 88 (1984) 1944.
- [9] J. Szczepanski, W. Personette, R. Pellow, T.M. Chandrasekhar, D. Roser, M. Cory, M. Zerner, M. Vala, *J. Chem. Phys.* 96 (1992) 35.
- [10] N.R. Daly, *Rev. Sci. Instrum.* 31 (1960) 264.
- [11] D. Gerlich, *Phys. Scr.* 59 (1995) 256.
- [12] S. Schlemmer, E. Lescop, J.V. Richthofen, D. Gerlich, M.A. Smith, *J. Chem. Phys.* 117 (2002) 2068.
- [13] D. Gerlich, *Adv. Chem. Phys.* 82 (1992) 1.
- [14] X. Tan, *Diatomic: a powerful spectral simulation program for diatomic molecules (TA01)*, The Ohio State University 57th International Symposium on Molecular Spectroscopy, Columbus, 2002.
- [15] X. Tan, *Diatomic, a spectral simulation program for diatomic molecules on Windows platforms*, Release 1.28 ed., 2004.
- [16] F. Muntean, L. Heumann, P.B. Armentrout, *J. Chem. Phys.* 116 (2002) 5593.
- [17] S. Olesik, T. Baer, J.C. Morrow, *J. Phys. Chem.* 90 (1986) 3563.
- [18] T. Sasaki, N. Mikami, *Chem. Phys. Lett.* 209 (1993) 379.
- [19] J.H.S. Green, *Spectrochim. Acta Part A* 26 (1970) 1503.
- [20] E.A. Rohlfing, C.M. Rohlfing, *J. Phys. Chem.* 93 (1989) 94.
- [21] W.D. Sands, R. Moore, *J. Phys. Chem.* 93 (1989) 101.